

Classification of cognitively normal controls, mild cognitive impairment and Alzheimer's disease using transfer learning approach

V.P. Subramanyam Rallabandi, K. Seetharaman^{*}, for the Alzheimer's Disease Neuroimaging Initiative (ADNI)¹

Dept. of Computer and Information Sciences, Annamalai University, Annamalai Nagar, Chidambaram, Tamil Nadu 608002, India

ARTICLE INFO

Keywords:

Transfer Learning
Balanced Random Forest
Diffusion tensor imaging
Diffusion kurtosis imaging
Fractional anisotropy
Mean diffusivity
White matter integrity

ABSTRACT

Automated classification of dementia stage using imaging will be useful for clinical diagnosis and the classification accuracy will be biased for highly imbalanced samples in each class. Hence, we propose a novel approach using transfer learning-based structural significance (TLSS) for the classification of cognitively normal controls (CN), mild cognitive impairment (MCI) and Alzheimer's disease (AD) patients based on white matter Gaussian diffusion (tensor) indices and non-Gaussian diffusion (kurtosis) indices. The structural T1-weighted magnetic resonance imaging and diffusion images were taken from ADNI dataset with 44 CN, 84 MCI and 22 AD patients. We estimate the regional Gaussian diffusion indices such as tensor fractional anisotropy (TFA) and mean diffusivity (TMD) as well as non-Gaussian diffusion indices such as kurtosis fractional anisotropy (KFA) and kurtosis mean diffusivity (KMD) in white matter regions. Further, we build transfer learning model using various balanced classifiers with structural expansion reduction (SER) and structure transfer using threshold (STT) and ensemble of majority voting of both SER and STT algorithms. We build two models by training the source model using kurtosis indices, refine the model on target tensor indices and vice versa. Transfer learning model using balanced random forest classifier was able to classify and predict all the groups with an overall accuracy about 0.79 using ensemble of SER and STT forests rather than individual algorithms (SER and STT). Our results conclude that the proposed model using kurtosis indices as source model classified and predicted with accuracies of 0.96, 0.72 and 0.7 in classifying CN vs AD, CN vs MCI and AD vs MCI respectively. To conclude, the proposed approach has improved the classification accuracy and its potential applicability for imbalanced data sample datasets.

Abbreviations: AD, Alzheimer's disease; ADNI, Alzheimer's disease neuroimaging initiative; ACR, Anterior corona radiate; ALIC, Anterior limb of internal capsule; AxD, Axial diffusivity; BRF, Balanced random forests; BCC, Body of corpus callosum; CP, Cerebellar peduncle; CDR-SB, Clinical dementia rating- sum of boxes; CN, Cognitive normal controls; CNN, Convolutional neural network; CR, Corona radiate; CST, Cortico-spinal tract; DL, Deep learning; DKI, Diffusion kurtosis imaging; DTI, Diffusion tensor imaging; DWI, Diffusion-weighted images; TE, Echo time; EC, External capsule; FX, Fornix; FX/ST, Fornix/ Stria terminalis; FA, Fractional anisotropy; FIC, Frontoinular cortex; fMRI, Functional MRI; GCC, Genu of corpus callosum; GM, Gray matter; HC, Hippocampal cingulum; IF, Inferiofrontal; IFO, Inferiofrontoorbital; TI, Inversion time; KNN, K-nearest neighbor; KFA, Kurtosis fractional anisotropy; KMD, Kurtosis mean diffusivity; MD, Mean diffusivity; ML, Medial lobe; MTG, Medial temporal gyrus; MF, Midfrontal; MCI, Mild cognitive impairment; MMSE, Mini-mental state examination; PVWM, Periventricular white matter; PCR, Posterior corona radiate; PLIC, Posterior limb of (internal capsule); PTR, Posterior thalamic radiation; RD, Radial diffusivity; RF, Random forests; ROS, Random oversampling; RUS, Random undersampling; RUSBoost, Random undersampling boosting; TR, Repetitive time; RFG, Right fusiform gyrus; SS, Sagittal status; SCC, Splenium of corpus callosum; SER, Structural Expansion and Reduction; sMRI, Structural Magnetic Resonance Imaging; STT, Structural Transfer with Thresholding; SGC, Subgenual cingulate cortex; SF, Superiorfrontal; SCR, Superior corona radiate; SLF, Superior longitudinal fasciculus; SFO, Superiorfrontoorbital; SMOTE, Synthetic minority over-sampling technique; TAP, Tapetum of corpus callosum; TFA, Tensor fractional anisotropy; TMD, Tensor mean diffusivity; TBSS, Tract-based spatial statistics; TLSS, Transfer learning-based structural significance; UNC, Uncinate fasciculus; WM, White matter.

^{*} Corresponding author.

E-mail address: kseethaddeau@gmail.com (K. Seetharaman).

¹ ADNI provided the data but neither involved in the study design nor data analysis.

<https://doi.org/10.1016/j.bspc.2022.104092>

Received 25 November 2021; Received in revised form 3 July 2022; Accepted 8 August 2022

Available online 22 August 2022

1746-8094/© 2022 Elsevier Ltd. All rights reserved.

1. Introduction

Dementia is a progressive decline in cognitive functioning such as memory, attention, language, and problem solving due to cortical cellular damage or neuro-degeneration in the brain when compared to healthy aging. Early detection of dementia stage will be helpful for efficacious treatment as delayed therapy will not be helpful in arresting the disease progression. Various structural magnetic resonance imaging (sMRI), diffusion-weighted imaging (DWI) and functional MRI (fMRI) techniques are available. However, diffusion tensor imaging (DTI) is a unique method to track the fiber pathways of anisotropic water diffusion in white matter (WM) neural fibers such as nerve, spine or brain. The water diffusion is sensitive to the underlying tissue microstructure that provides DTI of assessing the orientation and integrity of these neural fibers, which may be useful in several neurological disorders [1]. DTI is a Gaussian diffusion model ($k = 0$) for fluid and diffusion kurtosis imaging (DKI) is a non-Gaussian diffusion model for biological tissues which are characterized by a positive diffusion kurtosis ($k > 0$); whereas the latter shows potential in understanding of microstructure alternations in AD [2]. Quantitative indices will be more helpful rather than qualitative imaging and hence automated machine learning or deep learning (DL) models can be beneficial to improve classification accuracy.

DKI has been recently reported as a biomarker in classifying cognitive normal controls (CN), mild cognitive impairment (MCI) and Alzheimer's disease (AD) [3–5]. Few studies have reported distinct patterns of microstructural WM abnormalities in MCI and AD groups [6,7] including divergent topological networks in AD patients [8]. In addition, the WM integrity using tractography studies showed alterations in AD and MCI individuals [9,10,11]. Recently, a DTI study has been proposed to classify MCI and AD using WM integrity indices based on convolutional neural networks (CNNs) [12].

Several sMRI studies have been proposed using gray matter (GM) changes using tensor morphometry [13], independent component analysis [14] including DL classifiers using single slice sMRI [15] and cortical thickness features [16]. Recently, sMRI features such as gray matter density and local gyrification indices were derived and used the radial basis kernel-based support vector machine (SVM) classifier in classifying MCI, AD and CN [17]. A recent sMRI study using attention-guided deep-learning framework was proposed to extract multi-level discriminative stable MRI features for dementia diagnosis [18].

The multimodal imaging approaches have been proposed using sparse hierarchical extreme learning [19], sMRI and positron emission tomography (PET) studies [20]; multimodal fusion with DL [21–23]. Various DL-based fMRI studies have been proposed for early AD and MCI diagnosis [24], static and dynamic functional brain networks [25] spatiotemporal modeling and brain network hub detection [26,27]. A study using invariant and hierarchical features based on CNN on sMRI and resting state fMRI data [28]. Also, various DL methods using PET imaging [29] in classifying Parkinson's disease related dementia from AD patients including several PET studies in classifying CN, MCI and AD patients [30–33]. However, the main limitation of PET imaging is invasive and mainly dependent on glucose metabolism but reliability on PET studies for classifying MCI and CN is very less.

DL methods have been proposed to classify MCI and AD using electroencephalography (EEG) [34], brain asymmetry in the brain hemispheres of AD and MCI using deep Siamese neural networks [35], ensemble-based classification [36]. A study has been proposed using random forest feature selection and deep neural network classification strategy based on fuzzy logic learning on a mixed cohort including healthy and AD individuals [37]. A CNN model based on hippocampus [38], a classifier based on multiple cluster dense CNNs [39], CNN based approach based on cortical volume, surface area and cortical thickness features [40]. However, these DL models show good accuracy but they are black-box models meaning that they are complex systems and not able to interpret and identify the features. Also, DL models require huge training data, balanced samples in all groups which is a bottleneck in

medical imaging.

DTI tractography studies have showed significant decrease in fractional anisotropy (FA) of bilateral uncinate fasciculus and significant increase in radial diffusivity (RD) of left uncinate fasciculus with AD progression [41], increase in FA is found in crossing-fiber regions in MCI and AD and increase is due to the degeneration of secondary fibers in superior longitudinal fasciculus [42]. WM abnormalities have been noticed using ROI-based tractography [43], constrained spherical deconvolution approach [44] and disruption of WM integrity in CN, MCI and AD [45,46]. However, there are few issues in tractography about the curvature overshoot, termination, connection density and gyral biases and crossing-fiber issues.

To resolve the above limitations, we propose transfer learning-based structural significance (TLSS) and compare three algorithms such as structural expansion reduction (SER), applying structure transfer using thresholding (STT) and ensemble of both SER and STT forests (MIX) by training source model and refine it on target model with these three algorithms to classify CN, MCI and AD patients.

2. Methods

2.1. Image acquisition

The study included ADNI participants with 44 CN, 88 MCI and 23 AD patients and the demographic details are given in Table 1 along with the statistical significance ($p < 0.05$) between the groups using t -test in stats package python. All subjects underwent MRI brain scanning on 3 different scanners GE medical systems, Philips and Siemen scanners at different sites across North America. Structural T1-weighted anatomical scans were acquired using spoiled gradient echo sequences with 256×256 acquisition matrix; voxel size = $1.2 \times 1.0 \times 1.0 \text{ mm}^3$; inversion time (TI) = 400 ms; repetitive time (TR) = 6.98 ms; echo time (TE) = 2.85 ms; flip angle = 11° . The diffusion-weighted images (DWI) were acquired with multi-shell diffusion protocols using 256×256 matrix; voxel size = $2.0 \times 2.0 \times 2.0 \text{ mm}^3$; TR = 9000 ms; scan time = 9 min including 127 DWI volumes with 13 no diffusion sensitization b_0 images and 48 $b_1 = 1000 \text{ s/mm}^2$, 60 $b_2 = 2000 \text{ s/mm}^2$ (and excluded six $b = 500 \text{ s/mm}^2$) [47]. All the T1-weighted MR and DWI images were checked visually for quality assurance to exclude scans with excessive motion and/or artifacts. We excluded 4 MCI and 1 AD subject scans due to poor visual quality and artifacts. Detailed protocols are available at <https://adni.loni.usc.edu/methods/documents/mri-protocols/>.

Table 1
Demographic details of the study participants.

Group	CN	MCI	AD	CN vs MCI (p-value)	MCI vs AD (p-value)	CN vs AD (p-value)
Sample size (n)	44	84	22	—	—	—
Age (in years)	72.7 ± 5.9	74.1 ± 7.4	75.8 ± 10.0	0.531	0.765	0.513
Sex (M/F)	22 /22	50 /34	14 /8	—	—	—
Education (in years)	16.6 ± 2.7	16.2 ± 2.4	15.0 ± 3.0	0.368	0.663	0.873
MMSE	28.9 ± 1.3	27.9 ± 1.5	23.2 ± 1.7	9.58E-4	2.02E-23	1.61E-23
ADAS-cog score	5.6 ± 3.0	8.7 ± 4.1	18.9 ± 7.6	2.53E-5*	1.63E-14*	2.05E-15*
CDR-(sum of boxes)	0.03 ± 0.1	1.38 ± 0.7	4.96 ± 1.4	3.19E-23	4.01E-31	1.81E-31

* ADAS-cog score is available for CN = 41, MCI = 78 and AD = 20. Bold are significant ($p < 0.05$).

2.2. Pre-processing

For each subject, all raw DWI volumes were aligned to the average b_0 image DTI volume with no diffusion sensitization using the FSL *eddy_-correct* tool (<https://www.fmrib.ox.ac.uk/fsl>) to correct for head motion and eddy current distortions. Anatomical T1 scans were performed for intensity inhomogeneity normalization using the Montreal Neurological Institute (MNI) *nu_correct* tool (<https://www.bic.mni.mcgill.ca/software/>). Non-brain tissue was also removed from the anatomical T1 MRI and DWI images using the Brain Extraction Tool (BET) from FSL [48]. Skull-stripped volumes were visually inspected to avoid distorted or motion artifact images. To correct for echo-planar imaging induced susceptibility artifacts, which can cause distortions at tissue–fluid interfaces, skull-stripped b_0 images were linearly aligned (FSL *flirt12*) and then elastically registered to their respective T1-weighted anatomical MRI scans. Skull-stripped anatomical T1 images were non-linearly registered to a ICBM-152 T1 template using FSL *flirt* and warp the ICBM-152 template on to b_0 DTI space using FSL *fnirt* and then apply inverse warping to transform to native space [49]. We performed resampling of DWIs using B-spline interpolation. The resulting 3D deformation fields were then applied to the remaining all DWI volumes prior to estimating diffusion parameters using the DTI model. Finally, DTI images were non-linearly registered to ICBM template for WM segmentation, generate the scalar averaging of FA and MD maps and perform TLSS to find the significance between the groups. The entire preprocessing steps were shown in Fig. 1.

The predicted signal (S) relative to baseline signal (S_0) during application of Gaussian diffusion-sensitizing gradients can be expressed as.

$$S/S_0 = e^{-bA} \quad (1)$$

where A is apparent diffusion coefficient and b is scalar defining the strength of diffusion gradients.

Diffusion kurtosis tensors are extracted from diffusion tensors using.

$$S = S_0 e^{-bD + b^2 D^2 K / 6} \quad (2)$$

where D is the diffusion tensor and K is the kurtosis tensor.

DTI maps were generated using a single diffusion tensor or ellipsoid model [50] at each voxel in the brain from the eddy-corrected and echo planar imaging-corrected DWI scans using FSL *dtifit*, and obtained the diffusivity maps and scalar anisotropy from the resulting diffusion tensor eigenvalues ($\lambda_1, \lambda_2, \lambda_3$) which confines the length of the longest, middle, and shortest axes of the ellipsoid in which λ_1 is axial diffusivity (AxD), average of λ_2 and λ_3 is radial diffusivity (RD) and average of λ_1, λ_2 and λ_3 is defined as λ , mean diffusivity (MD) and FA defines the degree of anisotropy, a value between 0 (isotropic) and 1 (anisotropic) which is given by.

$$FA = \sqrt{\frac{3(\lambda_1 - \lambda)^2 + (\lambda_2 - \lambda)^2 + (\lambda_3 - \lambda)^2}{2(\lambda_1^2 + \lambda_2^2 + \lambda_3^2)}} \quad (3)$$

Diffusion kurtosis tensors are extracted from diffusion tensors using.

$$\ln S(b, n) = \ln(S_0) - b \sum_{ij} n_i n_j D_{ij} + \frac{b^2 \lambda}{6} \sum_{ijkl} n_i n_j n_k n_l K_{ijkl} \quad (4)$$

where S_0 is signal without diffusion weights, n is normalized direction unit vector, D is diffusion tensor, K is kurtosis tensor, λ is mean diffusivity and b is scalar defining the strength of diffusion gradients. For any

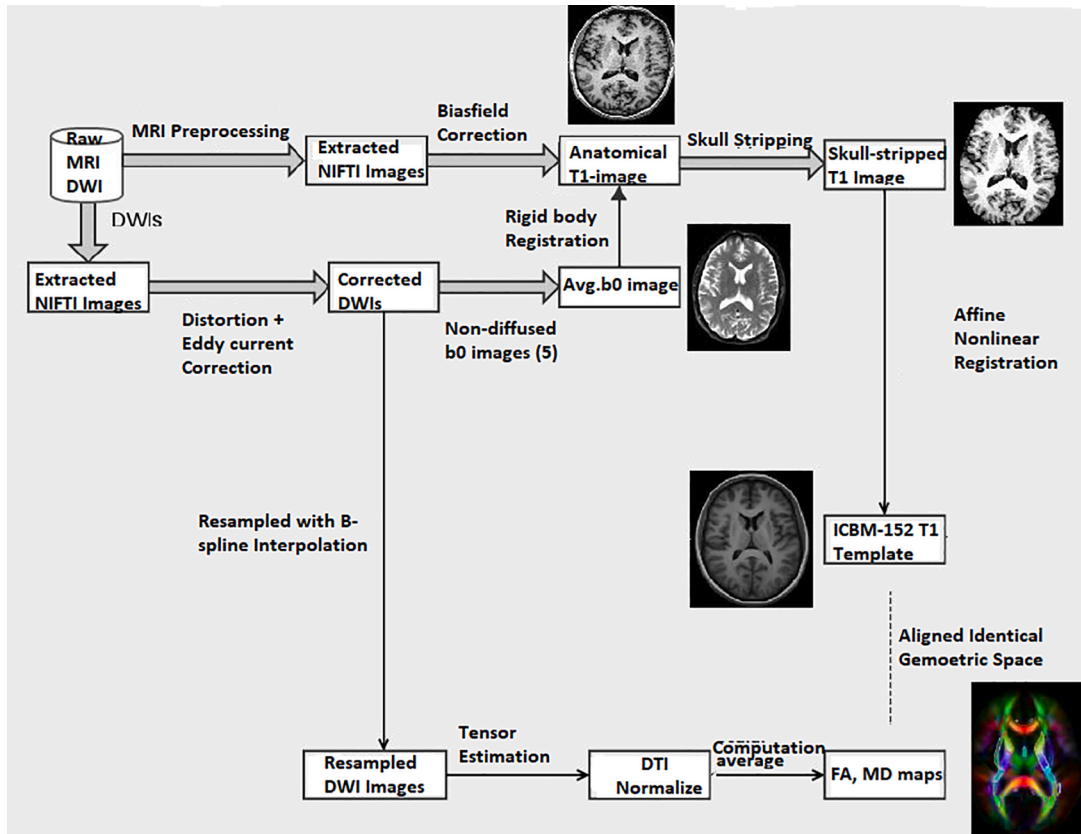


Fig. 1. Preprocessing steps for structural MRI anatomical T1 image using bias field correction, skull stripping, apply affine non-linear registration on skull-stripped T1 anatomical image on ICBM template; Preprocessing steps for DWI imaging: distortion and eddy current correction, resampled DWIs using B-spline interpolation, average b_0 image from non-directional b_0 images, tensor estimation, ICBM template registration to DTI in identical geometric space, normalization of DTI and compute scalar average FA and MD maps; and finally perform TLSS analysis.

arbitrary direction*, directional diffusion tensor and diffusion kurtosis are given by.

$$D(n) = \sum_{ij} n_i n_j D_{ij}^* \quad (5)$$

$$K(n) = \frac{\lambda^2}{D(n)^2} \sum_{i=1}^3 \sum_{j=1}^3 \sum_{k=1}^3 \sum_{l=1}^3 n_i n_j n_k n_l W_{ijkl}^* \quad (6)$$

The average diffusion tensor and kurtosis are measured by integrating across all directions $d(n)$ [51] using.

$$D(n) = \frac{1}{4\pi} \int d(n) D(n) \quad (7)$$

$$K(n) = \frac{1}{4\pi} \int d(n) K(n) \quad (8)$$

For white matter diffusion $k = 1$ will be considered. The DKI approach is an extension of the DTI, which has 9 parameters in total and only 6 parameters due to symmetry, whereas the full DKI model has 21 parameters in total: 15 independent parameters from the kurtosis model including 6 parameters from the original DTI model. The scalar diffusion kurtosis indices are calculated from these parameters using 3D rotational invariant similar to the diffusion indices in DTI and detailed mathematical calculation of the kurtosis indices was given in [52]. Then smoothing was done with a 3-mm full width at half maximum Gaussian kernel on motion-corrected diffusion data to generate DKI and fit to the diffusion kurtosis tensor model. Diffusion and kurtosis tensors are extracted using DiPy software [53,54]. In addition, direct linear squares will be used to evaluate diffusion tensor fractional anisotropy (TFA), and diffusion tensor mean diffusivity (TMD), kurtosis fractional anisotropy (KFA) and kurtosis mean diffusivity (KMD) by integrating across all the directions. The entire workflow of the proposed methodology is shown in Fig. 2.

2.3. Transfer learning-based structural significance

We have developed a transfer learning-based structural significance (TLSS) method using three different algorithms such as SER (Structural Expansion and Reduction), structural expansion of leaves and Recursive over child nodes). (Refer [supplementary file algorithm 1](#)), STT (Structural Transfer using Thresholding), refit thresholds using Gini coefficient (or index) until node impurity no longer decrease (Refer [supplementary file algorithm 2](#)) and MIX (is a simple majority voting applied over all decision trees transferred by either SER or STT methods (Refer [supplementary file algorithm 3](#))). We used Gini coefficient, the statistical measure of dispersion to identify significant differences between two groups (0 refers to no differences and higher score, 1

represents highly different). We evaluated these three algorithms with Gaussian diffusion features as source and non-Gaussian diffusion white matter indices as target and vice versa. Initially, we generate all the average tensor and kurtosis FA and MD maps among all the groups. We train these TFA and TMD features as source model and refine the target kurtosis model and similarly KFA and KMD features as source model and refine the target tensor model.

Since there is imbalance in the samples among all the groups, balanced random forest (BRF) considers equal samples from all the groups in training and rest will be assigned to test dataset. To handle imbalance class samples, currently existing methods are random over-sampling using synthetic minority oversampling technique, SMOTE [55] and undersampling classifiers like balanced bagging, easy ensemble and RUSBoost [56]. Since we have imbalance samples among three different groups such as CN, MCI and AD, the advantage of transfer learning using the balanced ensemble methods such as decision trees, random forests [57] for the feature selection obtained from the source (train) model and refine the features on target model to improve accuracy [58]. Also, the advantage of BRF [59] gives good balanced accuracy in classification due to unequal or imbalance in the sample size across groups rather than random oversampling and undersampling classifiers. We have implemented the BRF classifier using the imblearn package in python. Unlike traditional methods, where the models are over fitting to majority sample groups and the prediction results will be biased towards the majority class. However, BRF classifier considers equal sample size for training data among all the groups and hence the model does not overfit while testing which further improves the classification accuracy.

2.4. Hyperparameter optimization

Hyperparameter optimization will be helpful in learning and fine tuning the model by varying across different parameters [60]. The best hyper parameters for BRF classifier using grid search are number of estimators = 120, criteria = gini, max_depth = None, min_samples_split = 2, min_samples_leaf = 2, min_weight_fraction_leaf = 0, max_features = auto, max_leaf_nodes = None, min_impurity_decrease = 0.0, bootstrap = True, oob_score = False, sampling_strategy = auto, replacement = False. We then measured performance indices for imbalance dataset such as balanced accuracy (average of recall obtained for each class) and geometric mean (square root of product of specificity and sensitivity) and F1-score being the harmonic mean of precision and recall using the formulae given below.

$$\text{Specificity (or TNR)} = \text{TN} / (\text{FP} + \text{TN}) \quad (9)$$

$$\text{Precision} = \text{TP} / (\text{TP} + \text{FP}) \quad (10)$$

$$\text{Sensitivity or Recall (TPR)} = \text{TP} / (\text{TP} + \text{FN}) \quad (11)$$

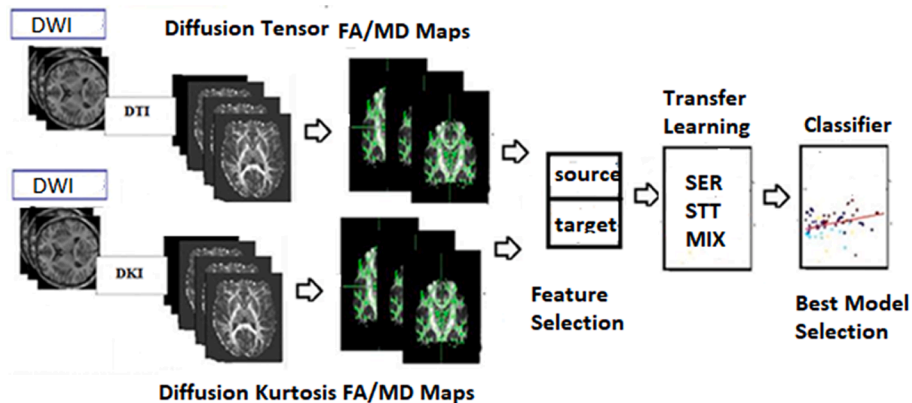


Fig. 2. Workflow of proposed transfer learning approach: generation of the diffusion tensor and kurtosis FA and MD from DWI images and train these tensor feature maps as source, kurtosis maps as target and vice versa using balanced classifiers to classify CN, MCI and AD patients.

$$\text{Accuracy} = (\text{TP} + \text{TN}) / (\text{TP} + \text{TN} + \text{FP} + \text{FN}) \quad (12)$$

$$F - \text{score} = 2 * \text{TP} / (2 * \text{TP} + \text{FP} + \text{FN}) \quad (13)$$

$$\text{Geometric Mean} = (\text{Specificity} * \text{Sensitivity})^{1/2} \quad (14)$$

where TP, FP, TN, FN are true positives, false positives, true negatives and false negatives respectively.

3. Results

The TLSS analysis for both tensor and kurtosis indices showed changes in various brain regions. Our TLSS model using tensor features (TFA and TMD) as the source and refined on target DKI, and kurtosis features (KFA and KMD) as source model and refine on target DTI were reported in Table 2 and Table 3 respectively. Our TLSS model analysis showed various brain regions that were highly significant different between the groups using the Gini coefficient between 0.9 and 1. From our results, we noticed that DTI as source model has fewer more regions significant than DKI as source model. Then we evaluated the TLSS model using SER, STT and MIX algorithms by considering TFA and TMD features as source model and refine on the target DKI model and compared various classifiers. Further, we evaluated the TLSS model using SER, STT and MIX algorithms by considering KFA and KMD features as the source model and refined on the target DTI model and compared various classifiers. The kurtosis as source model for MIX features using BRF classifier gives some common features from tensor as source model. We evaluated and compared all the three SER, STT and MIX algorithms using BRF classifier and achieved the highest performance for kurtosis as source and tensor as target rather than tensor as source and kurtosis as target. The area under the curve (AUC) for the source as kurtosis indices and target as tensor indices model; source as tensor indices and target as kurtosis indices using the best model (BRF classifier) are 0.81 and 0.7 respectively. Furthermore, we noticed that the overall accuracy and geometric mean scores were better for kurtosis indices than diffusion indices model. From comparison of all the model results, we noticed that TLSS model with MIX method using source as DKI and target as DTI features achieved the highest overall accuracy and geometric mean and outperformed the other methods SER and STT for 5-fold cross-validation as given in Table 4.

Usually for imbalance class samples, balanced accuracy, F1-score and geometric mean were considered as performance indices. Balanced accuracy of 0.79 and geometric mean of 0.78 using BRF classifier was obtained for kurtosis indices as source model and tensor

Table 2
Diffusion tensor regional changes using TLSS and comparison in various groups.

CN vs AD	Gini Index	CN vs MCI	Gini Index	MCI vs AD	Gini Index
L&R FX/ST	0.98, 0.93	L&R HC	0.98, 0.94	L&R FX/ST	0.98, 0.92
Left HC	0.97	Left SCC	0.96	Left HC	0.98
Left TAP	0.96	Left TAP	0.94	Left ACR	0.97
L&H SCC	0.96	L&R FX/ST	0.93, 0.91	Left SFO	0.96
Left BCC	0.95	Left ACR	0.92	Left SCC	0.95
Left SFO	0.95	Left SLF	0.91	Left TAP	0.94
Left ACR	0.94			Left PTR	0.94
Left PTR	0.94			Left BCC	0.94
Left CP	0.93			Left SS	0.93
Left SS	0.93			Left GCC	0.93
Left SCR	0.93			Left UNC	0.93
Left IFO	0.92			Left CP	0.92
Left UNC	0.92			Left ALIC	0.92
Left PCR	0.92			Left RLIC	0.91
Left GCC	0.92			Left CST	0.91
Left SLF	0.92			Left EC	0.91
Left CST	0.92			Left SLF	0.91
Left EC	0.91				
Left RLIC	0.91				
Left ALIC	0.91				

Table 3

Diffusion kurtosis regional changes using TLSS and comparison in various groups.

CN vs AD	Gini Index	CN vs MCI	Gini Index	MCI vs AD	Gini Index
Left HC	0.98	Left HC	0.98	Left HC	0.98
L&R FX/ST	0.98, 0.92	L&R SCC	0.97, 0.91	L&R SCC	0.98, 0.92
L&R SCC	0.97, 0.91	L&R FX/ST	0.96, 0.93	Left FX/ST	0.97
Left BCC	0.96	Left SLF	0.95	Left SLF	0.96
Left PTR	0.95	Left PCR	0.94	Left ACR	0.95
Left SLF	0.95	Left ACR	0.92	Left BCC	0.95
Left ACR	0.94	Left EC	0.91	Left PCR	0.94
Left UNC	0.94			Left PTR	0.93
Left PCR	0.93			Left UNC	0.92
Left SCR	0.93			Left EC	0.92
Left EC	0.92			Left IFO	0.91
Left IFO	0.91				

Table 4

Comparison of performance indices for source and target models with different methods using random oversampling and undersampling classifiers.

ML Classifier	Overall Accuracy	Specificity	Sensitivity	F1-score	Geometric Mean
Source: DKI; Target: DTI					
STT_BRF	0.7	0.72	0.71	0.65	0.7
SER_BRF	0.67	0.66	0.68	0.62	0.66
MIX_BRF	0.79	0.81	0.78	0.7	0.78
Balanced	0.69	0.67	0.6	0.68	0.68
Bagging					
Easy Ensemble	0.69	0.68	0.7	0.65	0.7
SMOTE_KNN	0.7	0.71	0.69	0.61	0.7
RUSBoost	0.69	0.71	0.6	0.61	0.69
Source: DTI; Target: DKI					
STT_BRF	0.63	0.64	0.62	0.59	0.62
SER_BRF	0.62	0.61	0.63	0.6	0.62
MIX_BRF	0.73	0.74	0.71	0.64	0.72
Balanced	0.59	0.58	0.59	0.56	0.58
Bagging					
Easy Ensemble	0.6	0.6	0.61	0.58	0.6
SMOTE_KNN	0.61	0.61	0.61	0.59	0.61
RUSBoost	0.62	0.61	0.6	0.59	0.62

indices as target and the classification accuracies of CN vs AD, CN vs MCI and CN vs MCI are 0.96, 0.72 and 0.7 respectively. The balanced accuracy of 0.73 and geometric mean of 0.72 was achieved for tensor indices as source model and kurtosis indices as target and the classification accuracies of CN vs AD, CN vs MCI and CN vs MCI are 0.86, 0.7 and 0.63 respectively. The receiver operating characteristic (ROC) plot infers the tradeoff between false positive rate on x-axis and true positive rate on y-axis at different thresholds showing the area under the curve as a performance measure. The ROC plots were shown for CN, MCI and AD using one vs rest (one group as TPs versus other groups as TNs) and predict FPs and FNns using the best model. We found that MIX_BRF is the best model for source DTI and target DKI as well as source DKI and target DTI were shown in Fig. 3 (A) and (B) respectively.

4. Discussion

Several diffusion imaging studies reported brain regions in classifying normal aging, MCI and AD using tract-based spatial statistics (TBSS) [61,62] and tract-based network connectivity [63]. Our results are also consistent with these studies that reported the changes in the hippocampal region of cingulum, splenium of corpus callosum. Our results were consistent with a DKI study that reported splenium of corpus callosum and corona radiata regions involvement in classification of MCI and AD [64]. Our BRF classifier also identified these regions and our results are consistent with TBSS and ROI tractography approaches. Recently, various feature selection methods such as low-level features (LLF) and SAE-learned Feature representation (SAEF) using DL have

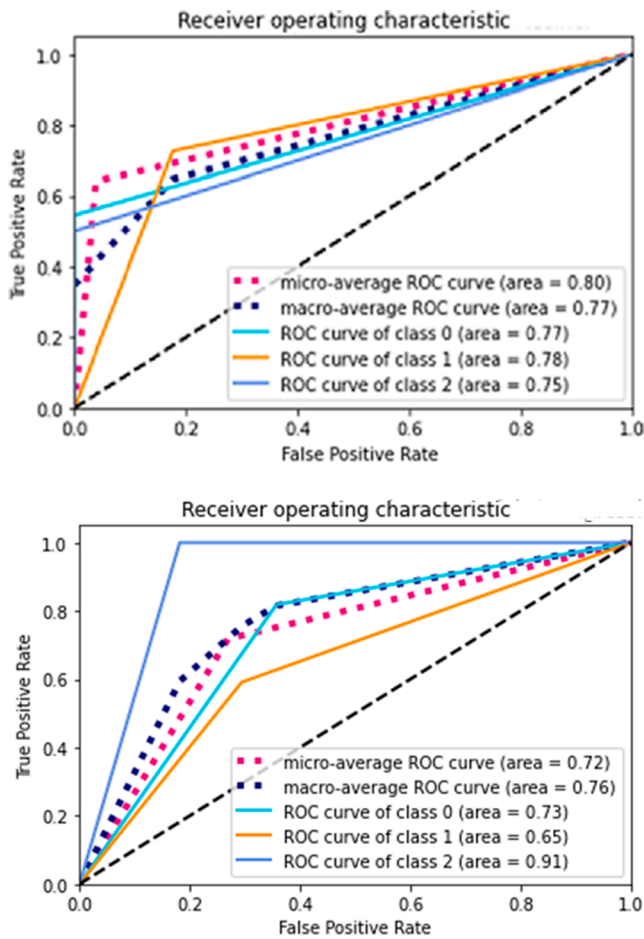


Fig. 3. ROC plots for one vs rest using the best model MIX_BRF for (A) Source DTI and Target DKI; (B) Source DKI and Target DTI. (class 0: CN; class 1: MCI and class 2: AD).

been proposed in classifying AD/CN, MCI/CN and MCI/AD by combining MRI features from GM volumes and PET features as mean signal intensities [65], latent features using stacked autoencoder approach [66] and sparse multi-task learning [67].

Although the DL models showed good classification accuracy, these models are black-box models and not able to predict the regions responsible for the pathological changes. In the case of multimodal studies, the same number of samples in each group for all modalities are not available and hence difficult to train DL models due to less samples data. Hence most of these DL models used to generate the synthetic samples using data augmentation techniques like generative adversarial network and hence not feasible for clinical utility due to the lack of diverse samples. Also, there will be issues in image decomposition using fMRI and sMRI data.

The limitations of diffusion tractography are tackling the curvature overshoot, termination, connection density and gyral biases and false positive errors that are produced in conventional or raw tractography algorithms and require correction methods. Also, there exist many other possible manifestations of such biases and errors, traverse part of one bundle and part of another, producing trajectories that are not present in the underlying structure [68]. The ill-posed nature of streamline terminations has been addressed by utilizing anatomical reference data to impose relevant prior information using Anatomically Constrained Tractography (ACT) and similar kind of framework to handle streamline tractography and termination [69–71]. The number of structural connection trajectories were consistent between the number of such reconstructed connections with the density of those underlying fibers (i. e., the actual number of axons in a white matter region) [72]. Gyral bias

is basically the termination ends at gyri rather than sulci [73,74]. The source of the gyral bias is multifactorial, such as the complexity of axon arrangement at the junction of cortical grey matter and superficial white matter [75]. The partial volume effect from the limited MRI spatial resolution introduces difficulties in distinguishing complex fiber configurations based on the reconstructed fiber orientation distributions and it can be avoided by increasing the resolution of the images.

Recent studies suggested that performance of filtering methods can be significantly boosted by combining *knowledge-* and *data-driven* strategies. These new formulations [76,77] allow taking explicitly into account two fundamental assumptions about the connections in the brain: (i) fibers are naturally organized in bundles [78] and (ii) number of bundles should be low to minimize the overall wiring cost [79]. In addition, manual inclusion of the regions-of-interest (ROIs usually chosen in the gray matter cortical and subcortical structures) to define constraint where the streamlines should terminate in WM, define where the streamlines should pass, and exclusion ROIs are placed in other regions to exclude undesired streamlines [80,81]. Manual streamline selection is considered to be the gold standard to delineate anatomical fiber tracts in tractography especially in clinical utility for presurgical white matter mapping in tumor patients in which tumor or lesion can largely displace the WM fiber tracts.

There are few challenges involved in DKI like estimation of a large number of parameters and also very sensitive to the noise or artefacts. Since the non-Gaussian components of the diffusion signal are more sensitive to artefacts [82], it might be favorable to suppress the effects of noise and artefacts before diffusional kurtosis fitting. Noise in the imaging datasets were suppressed using denoising algorithms like PCA [83], Gibbs ringing artefacts were attenuated using a sub-voxel Fourier transform shifts [84] to provide optimal performances for DKI [85,86].

The main advantages of the proposed method over existing methods were firstly, low feature dimensionality derived on diffusion tensor and kurtosis features compared to structural T1-weighted and functional imaging modalities. For instance, where one modality has many more features than another (or has variation on a much larger scale), classification algorithms trained on concatenated features may produce prediction models that effectively ignore the other modalities. Secondly, the misregistration error of 3D MRI and PET imaging as well as image decomposition issues on structural MRI to 4D fMRI data. Thirdly, most of the DL-based imaging studies do not report handling of imbalanced samples in each group and usually perform data augmentation technique using random combinations of intensity variation, rotation, translation, horizontal and vertical flipping methods to avoid model overfitting or underfitting. In this study, we developed an approach to handle imbalanced data samples and avoid model overfitting or underfitting. Lastly, the proposed method is *knowledge-* and *data-driven* approach and hence may be applicable to the other modalities as well. However, there are few limitations in our study. Firstly, the prediction of disease progression or conversion back or stable over time (longitudinal data). Also, DKI requires huge computational power which is expensive and complex for estimation of parameters. In particular, our model requires more than 3 nodes (or regions) for branching and implementation of SER and STT algorithms. Current understanding of imaging biomarkers for AD are limited for clinical utility and hence needed novel imaging methods to overcome the current limitations. Thus, transfer learning model have achieved good classification accuracy for imbalanced data samples and can be helpful for AD diagnosis.

5. Conclusions

We developed a transfer learning-based structural significance approach by training with source model and refine it on target model. Transfer learning using three algorithms with kurtosis KFA and KMD as source model and refined on target model TFA and TMD showed good performance. From this study, we conclude that the transfer learning using a balanced random forest classifier with MIX algorithm for source

as kurtosis indices and target as tensor indices achieved the best overall accuracy of 0.79 when compared to existing methods, individual models such as SER and STT. To conclude, transfer learning model have improved the classification accuracy compared to traditional ML models for imbalanced data sample dataset using combination of diffusion tensor and kurtosis quantitative indices and their reliability under test–retest conditions.

Author contributions

VPSR implemented the algorithms and performed data analysis. VPSR and KS design the study and wrote the manuscript.

Declaration of Competing Interest

The authors declare that they have no known competing financial interests or personal relationships that could have appeared to influence the work reported in this paper.

Data availability

The authors do not have permission to share data.

Acknowledgments

Data collection and sharing for this project was funded by ADNI (NIH Grant [U01 AG024904](#), [P30 AG010129](#) and [K01 AG030514](#)). ADNI is funded by the National Institute on Aging, the National Institute of Biomedical Imaging and Bioengineering, and through generous contributions from the following: Abbott; Alzheimer’s Association; Alzheimer’s Drug Discovery Foundation; Amorfix Life Sciences Ltd.; AstraZeneca; Bayer HealthCare; BioClinica, Inc.; Biogen Idec Inc.; Bristol-Myers Squibb Company; Eisai Inc.; Elan Pharmaceuticals Inc.; Eli Lilly and Company; F. Hoffmann-La Roche Ltd. and its affiliated company Genentech, Inc.; GE Healthcare; Innogenetics, N.V.; IXICO Ltd.; Janssen Alzheimer [Immunotherapy](#) Research & Development, LLC.; Johnson & Johnson Pharmaceutical Research & Development LLC.; Medpace, Inc.; Merck & Co., Inc.; Meso Scale Diagnostics, LLC.; Novartis Pharmaceuticals Corporation; Pfizer Inc.; Servier; Synarc Inc.; and Takeda Pharmaceutical Company. The Canadian Institutes of Health Research is providing funds to support ADNI clinical sites in Canada. Private sector contributions are facilitated by the Foundation for the National Institutes of Health ([www.fnih.org](#)). The grantee organization is the Northern California Institute for Research and Education, and the study is coordinated by the [Alzheimer’s Disease](#) Cooperative Study at the University of California, San Diego. ADNI data are disseminated by the Laboratory for Neuro Imaging at the University of California, Los Angeles. Investigators within ADNI contributed to the design and implementation of ADNI and/or provided data but did not participate in the analysis or writing of this report. The complete list of ADNI investigators are available at https://adni.loni.usc.edu/wp-content/uploads/how_to_apply/ADNI_Authorship_List.pdf. Also, we would like to thank anonymous reviewers for their valuable suggestions and comments to improve this manuscript.

Appendix A. Supplementary material

Supplementary data to this article can be found online at <https://doi.org/10.1016/j.bspc.2022.104092>.

References

[1] M. Bozzali, A. Cherubini, Diffusion tensor MRI to investigate dementias: a brief review, *Magn. Reson. Imaging* 25 (2007) 969–977, <https://doi.org/10.1016/j.mri.2007.03.017>.

[2] L. Yuan, M. Sun, Y. Chen, M. Long, X. Zhao, J. Yin, X.u. Yan, D. Ji, H. Ni, Non-Gaussian diffusion alterations on diffusion kurtosis imaging in patients with early Alzheimer’s disease, *Neurosci. Lett.* 616 (2016) 11–18.

[3] Y. Xue, Z. Zhang, C. Wen, H. Liu, S. Wang, J. Li, Q. Zhuge, W. Chen, Q. Ye, Characterization of Alzheimer’s Disease using ultra-high b-values apparent diffusion coefficient and diffusion kurtosis imaging, *Aging Dis.* 10 (5) (2019) 1026.

[4] J. Praet, N.V. Manyakov, L. Muchene, Z. Mai, V. Terzopoulos, S. de Backer, A. n. Torremans, P.-J. Gans, T. Van De Castele, A. Bittelbergs, B. Van Broeck, J. Sijbers, D. Smeets, Z. Shkedy, L. Bijmens, D.J. Pemberton, M.E. Schmidt, A. Van der Linden, M. Verhoye, Diffusion kurtosis imaging allows the early detection and longitudinal follow-up of amyloid- β -induced pathology, *Alzheimers Res. Ther.* 10 (1) (2018), <https://doi.org/10.1186/s13195-017-0329-8>.

[5] G.P. Song, T.T. Yao, D. Wang, Y.H. Li, Differentiating between Alzheimer’s disease, amnesic mild cognitive impairment and normal aging via diffusion kurtosis imaging, *Neural Regen. Res.* 14 (2019) 2141–2146, <https://doi.org/10.4103/1673-5374.262594>.

[6] F. Ji, O. Pasternak, S. Liu, et al., Distinct white matter microstructural abnormalities and extracellular water increases relate to cognitive impairment in Alzheimer’s disease with and without cerebrovascular disease, *Alzheimers. Res. Ther.* 9 (2017), <https://doi.org/10.1186/s13195017-0292-4>.

[7] N.J. Gong, C.C. Chan, L.M. Leung, et al., Differential microstructural and morphological abnormalities in mild cognitive impairment and Alzheimer’s disease: evidence from cortical and deep gray matter, *Hum. Brain Mapp.* 38 (2017) 2495–2508, <https://doi.org/10.1002/hbm.23535>.

[8] J.-X. Cheng, H.-Y. Zhang, Z.-K. Peng, Y. Xu, H. Tang, J.-T. Wu, J. Xu, Divergent topological networks in Alzheimer’s disease: a diffusion kurtosis imaging analysis, *Transl. Neurodegener.* 7 (1) (2018), <https://doi.org/10.1186/s40035-018-0115-y>.

[9] G.R. Glenn, L.-W. Kuo, Y.-P. Chao, C.-Y. Lee, J.A. Helpert, J.H. Jensen, Mapping the orientation of white matter fiber bundles: a comparative study of diffusion tensor imaging, diffusional kurtosis imaging, and diffusion spectrum imaging, *Am. J. Neuroradiol.* 37 (7) (2016) 1216–1222.

[10] E. Fieremans, A. Benitez, J.H. Jensen, M.F. Falangola, A. Tabesh, R.L. Deardorff, M. V.S. Spampinato, J.S. Babb, D.S. Novikov, S.H. Ferris, J.A. Helpert, Novel white matter tract integrity metrics sensitive to Alzheimer disease progression, *Am. J. Neuroradiol.* 34 (11) (2013) 2105–2112.

[11] Q. Wen, S.M. Mustafa, J. Li, S.L. Risacher, E. Tallman, S.A. Brown, J.D. West, J. Harezlak, M.R. Farlow, F.W. Unverzagt, S. Gao, L.G. Apostolova, A.J. Saykin, Y.-C. Wu, White matter alterations in early-stage Alzheimer’s disease: a tract-specific study, *Alzheimers Dement (Amst)* 11 (1) (2019) 576–587.

[12] E.N. Marzban, A.M. Eldeib, I.A. Yassine, Y.M. Kadah, S.D. Ginsberg, Alzheimer’s disease diagnosis from diffusion tensor images using convolutional neural networks, *PLoS One* 15 (3) (2020) e0230409.

[13] T. Tuokkola, M. Karrasch, J. Koikkalainen, R. Parkkola, J. Lötjönen, E. Löttyntiemi, S. Hurme, J. Rinne, Association between deep gray matter changes and neurocognitive function in mild cognitive impairment and Alzheimer’s disease: a tensor-based morphometric MRI study, *Dement Geriatr. Cogn. Disord.* 48 (1–2) (2019) 68–78.

[14] S. Basheera, M.S. Sai Ram, Convolution neural network-based Alzheimer’s disease classification using hybrid enhanced independent component analysis based segmented gray matter of T2 weighted magnetic resonance imaging with clinical valuation, *Alzheimers Dement. (NY)* 5 (2019) 974–986, <https://doi.org/10.1016/j.trci.2019.10.001>.

[15] S. Basaia, F. Agosta, L. Wagner, E. Canu, G. Magnani, R. Santangelo, M. Filippi, Automated classification of Alzheimer’s disease and mild cognitive impairment using a single MRI and deep neural networks, *Neuroimage Clin.* 21 (2019) 101645.

[16] V.P.S. Rallabandi, K. Tulpule, M. Gattu, Automatic classification of cognitively normal, mild cognitive impairment and Alzheimer’s disease using structural MRI analysis, *Informatics Medicine Unlocked* (2020) 100305.

[17] V.P.S. Rallabandi, K. Seetharaman, Machine Learning-Based Classification of Dementia Types: MRI Study, *IEEE International Conference on Artificial Intelligence and Smart Systems (ICAIS)* (2021) 109–114, <https://doi.org/10.1109/ICAIS50930.2021.9395957>.

[18] C. Lian, M. Liu, Y. Pan, D. Shen, Attention-guided hybrid network for dementia diagnosis with structural MR images, *IEEE Trans. Cybern.* 52 (4) (2022) 1992–2003.

[19] J. Kim, B. Lee, Identification of Alzheimer’s disease and mild cognitive impairment using multimodal sparse hierarchical extreme learning machine, *Hum. Brain Mapp.* 39 (2018) 3728–3741, <https://doi.org/10.1002/hbm.24207>.

[20] D. Lu, K. Popuri, G.W. Ding, R. Balachandrar, M.F. Beg, Multimodal and multiscale deep neural networks for the early diagnosis of Alzheimer’s disease using structural MR and FDG-PET images, *Sci. Rep.* 8 (1) (2018), <https://doi.org/10.1038/s41598-018-22871-z>.

[21] H.I. Suk, S.W. Lee, D. Shen, Alzheimer’s Disease Neuroimaging Initiative, Hierarchical feature representation and multimodal fusion with deep learning for AD/MCI diagnosis, *Neuroimage* 10 (2014) 569–582, <https://doi.org/10.1016/j.neuroimage.2014.06.077>.

[22] T. Zhou, K.H. Thung, X. Zhu, D. Shen, Effective feature learning and fusion of multimodality data using stage-wise deep neural network for dementia diagnosis, *Hum. Brain Mapp.* 40 (2019) 1001–1016, <https://doi.org/10.1002/hbm.24428>.

[23] C. Ieracitano, N. Mammone, A. Hussain, F.C. Morabito, A novel multi-modal machine learning based approach for automatic classification of EEG recordings in dementia, *Neural Netw.* 123 (2020) 176–190.

[24] T.E. Kam, H. Zhang, D. Shen, A novel deep learning framework on brain functional networks for early MCI diagnosis, *Med. Image Comput. Comput. Assist. Interv.* 11072 (2018) 293–301, https://doi.org/10.1007/978-3-030-00931-3_34.

- [25] T.E. Kam, H. Zhang, Z. Jiao, D. Shen, Deep learning of static and dynamic brain functional networks for early MCI detection, *IEEE Trans. Med. Imaging* 39 (2020) 478–487, <https://doi.org/10.1109/TMI.2019.2928790>.
- [26] M. Wang, C. Lian, D. Yao, D. Zhang, M. Liu, D. Shen, Spatial-temporal dependency modeling and network hub detection for functional MRI analysis via convolutional-recurrent network, *IEEE Trans. Biomed. Eng.* 67 (8) (2020) 2241–2252.
- [27] D. Yang, R. Huang, S.-H. Yoo, M.-J. Shin, J.A. Yoon, Y.-I. Shin, K.-S. Hong, Detection of mild cognitive impairment using convolutional neural network: Temporal-feature maps of functional near-infrared spectroscopy, *Front. Aging Neurosci.* 12 (2020), <https://doi.org/10.3389/fnagi.2020.00141>.
- [28] S. Sarraf, D.D. Desouza, J.A.E. Anderson, C. Saverino, MCADNet: recognizing stages of cognitive impairment through efficient convolutional fMRI and MRI neural network topology models, *IEEE Access* 7 (2019) 155584–155600.
- [29] H. Choi, Y.K. Kim, E.J. Yoon, J.-Y. Lee, D.S. Lee, Cognitive signature of brain FDG PET based on deep learning: domain transfer from Alzheimer's disease to Parkinson's disease, *Eur. J. Nucl. Med. Mol. Imaging* 47 (2) (2020) 403–412.
- [30] S. Singh, A. Srivastava, L. Mi, et al., Deep Learning based classification of FDG-PET data for Alzheimer's disease categories, *Proc. SPIE Int. Soc. Opt. Eng.* 10572 (2017) 105720J, <https://doi.org/10.1117/12.2294537>.
- [31] M. Liu, D. Cheng, W. Yan, Classification of Alzheimer's disease by combination of convolutional and recurrent neural networks using FDG-PET images, *Front. Neuroinform.* 12 (2018) 35, <https://doi.org/10.3389/fninf.2018.00035>.
- [32] D. Lu, K. Popuri, G.W. Ding, R. Balachandrar, M.F. Beg, Multiscale deep neural network based analysis of FDG-PET images for the early diagnosis of Alzheimer's disease, *Med. Image Anal.* 46 (2018) 26–34.
- [33] T. Shen, J. Jiang, J. Lu, M. Wang, C. Zuo, Z. Yu, Z. Yan, Predicting Alzheimer disease from mild cognitive impairment with a deep belief network based on ¹⁸F-FDG-PET images, *Mol. Imaging* 18 (2019), <https://doi.org/10.1177/1536012119877285>, 1536012119877285.
- [34] D. Kim, K. Kim, Detection of early-stage Alzheimer's disease using EEG relative power with deep neural network, *Conf. Proc. IEEE Eng. Med. Biol. Soc.* (2018) 352–355, <https://doi.org/10.1109/EMBC.2018.8512231>.
- [35] C.-F. Liu, S. Padhy, S. Ramachandran, V.X. Wang, A. Efimov, A. Bernal, L. Shi, M. Vaillant, J.T. Ratnanather, A.V. Faria, B. Caffo, M. Albert, M.I. Miller, Using deep Siamese neural networks for detection of brain asymmetries associated with Alzheimer's disease and mild cognitive impairment, *Magn. Reson. Imaging* 64 (2019) 190–199.
- [36] A. Ortiz, J. Munilla, J.M. Górriz, J. Ramírez, Ensembles of deep learning architectures for the early diagnosis of the Alzheimer's disease, *Int. J. Neural. Syst.* 26 (07) (2016) 1650025.
- [37] N. Amoroso, D. Diacono, A. Fanizzi, M. La Rocca, A. Monaco, A. Lombardi, C. Guaragnella, R. Bellotti, S. Tangaro, Deep learning reveals Alzheimer's disease onset in MCI subjects: results from an international challenge, *J. Neurosci. Methods* 302 (2018) 3–9.
- [38] M. Liu, F. Li, H. Yan, K. Wang, Y. Ma, L. Shen, M. Xu, A multi-model deep convolutional neural network for automatic hippocampus segmentation and classification in Alzheimer's disease, *Neuroimage* 208 (2020) 116459.
- [39] F. Li, M. Liu, Alzheimer's disease diagnosis based on multiple cluster dense convolutional networks, *Comput. Med. Imaging Graph.* 70 (2018) 101–110, <https://doi.org/10.1016/j.compmedimag.2018.09.009>.
- [40] W. Lin, T. Tong, Q. Gao, D. Guo, X. Du, Y. Yang, G. Guo, M. Xiao, M. Du, X. Qu, Convolutional neural networks-based MRI image analysis for the Alzheimer's disease prediction from mild cognitive impairment, *Front. Neurosci.* 12 (2018), <https://doi.org/10.3389/fnins.2018.00777>.
- [41] S. Kitamura, K. Kiuchi, T. Taoka, K. Hashimoto, S. Ueda, F. Yasuno, M. Morikawa, K. Kichikawa, T. Kishimoto, Longitudinal white matter changes in Alzheimer's disease: a tractography-based analysis study, *Brain Res.* 1515 (2013) 12–18.
- [42] G. Douaud, S. Jbabdi, T.E.J. Behrens, R.A. Menke, A. Gass, A.U. Monsch, A. Rao, B. Whitcher, G. Kindlmann, P.M. Matthews, S. Smith, DTI measures in crossing-fibre areas: increased diffusion anisotropy reveals early white matter alteration in MCI and mild Alzheimer's disease, *NeuroImage* 55 (3) (2011) 880–890.
- [43] B. Bigham, S.A. Zamanpour, F. Zemorshidi, F. Boroumand, H. Zare, Identification of superficial white matter abnormalities in Alzheimer's Disease and mild cognitive impairment using diffusion tensor imaging, *ADR* 4 (1) (2020) 49–59.
- [44] Y.D. Reijmer, A. Leemans, S.M. Heringa, I. Wieleaard, B. Jeurissen, H.L. Koek, G. J. Biessels, W. Zhan, Improved sensitivity to cerebral white matter abnormalities in Alzheimer's disease with spherical deconvolution based tractography, *PLoS ONE* 7 (8) (2012) e44074.
- [45] J. Gao, R.-F. Cheung, T.M.C. Lee, L.-W. Chu, Y.-S. Chan, H.-F. Mak, J.X. Zhang, D. Qiu, G. Fung, C. Cheung, Possible retrogenesis observed with fiber tracking: an anteroposterior pattern of white matter disintegrity in normal aging and Alzheimer's Disease, *JAD* 26 (1) (2011) 47–58.
- [46] A.C. Bozoki, I.O. Korolev, N.C. Davis, L.A. Hoisington, K.L. Berger, Disruption of limbic white matter pathways in mild cognitive impairment and Alzheimer's disease: a DTI/FDG-PET study, *Hum. Brain Mapp.* 33 (8) (2012) 1792–1802.
- [47] A. Zavaliangos-Petropulu, T.M. Nir, S.I. Thomopoulos, R.I. Reid, M.A. Bernstein, B. Borowski, C.R. Jack Jr., M.W. Weiner, N. Jahanshad, P.M. Thompson, Diffusion MRI indices and their relation to cognitive impairment in brain aging: the updated multi-protocol approach in ADNI3, *Front. Neuroinform.* 13 (2019) 2.
- [48] S.M. Smith, M. Jenkinson, M.W. Woolrich, C.F. Beckmann, T.E.J. Behrens, H. Johansen-Berg, P.R. Bannister, M. De Luca, I. Drobniak, D.E. Flitney, R.K. Niazy, J. Saunders, J. Vickers, Y. Zhang, N. De Stefano, J.M. Brady, P.M. Matthews, Advances in functional and structural MR image analysis and implementation as FSL, *NeuroImage* 23 (2004) S208–S219.
- [49] M. Jenkinson, P. Bannister, M. Brady, S. Smith, Improved optimization for the robust and accurate linear registration and motion correction of brain images, *Neuroimage* 17 (2002) 825–841, <https://doi.org/10.1006/nimg.2002.1132>.
- [50] P.J. Basser, J. Mattiello, D. LeBihan, MR diffusion tensor spectroscopy and imaging, *Biophys. J.* 66 (1) (1994) 259–267.
- [51] J.H. Jensen, J.A. Helpert, A. Ramani, H. Lu, K. Kaczynski, Diffusional kurtosis imaging: the quantification of non-gaussian water diffusion by means of magnetic resonance imaging, *Magn. Reson. Med.* 53 (6) (2005) 1432–1440.
- [52] B. Hansen, N. Shemesh, S.N. Jespersen, Fast imaging of mean, axial and radial diffusion kurtosis, *NeuroImage* 142 (2016) 381–393.
- [53] G.R. Glenn, J.A. Helpert, A. Tabesh, J.H. Jensen, Quantitative assessment of diffusional kurtosis anisotropy, *NMR Biomed.* 28 (4) (2015) 448–459.
- [54] R.N. Henriques, M.M. Correia, M. Marrale, E. Huber, J. Kruper, S. Koudoro, J. D. Yeatman, E. Garyfallidis, A. Rokem, Diffusional kurtosis imaging in the diffusion imaging in python project, *Front. Hum. Neurosci.* 15 (2021), <https://doi.org/10.3389/fnhum.2021.675433>.
- [55] N.V. Chawla, K.W. Bowyer, et al., SMOTE: Synthetic minority over-sampling technique, *J. Artif. Intell. Res.* 16 (2002) 321–357. <https://arxiv.org/pdf/1106.1813.pdf>.
- [56] C. Seiffert, T.M. Khoshgoftaar, J. Van Hulse, A. Napolitano, RUSBoost: A hybrid approach to alleviating class imbalance, *IEEE Trans. Syst. Man, Cybern.-Part A: Syst. Hum.* 40 (1) (2010) 185–197.
- [57] L. Breiman, Random Forests, *Mach. Learn.* 45 (2001) 5–32, <https://doi.org/10.1023/A:1010933404324>.
- [58] N. Segev, M. Harel, S. Mannor, K. Crammer, R. El-Yaniv, Learn on source, refine on target: a model transfer learning framework with random forests, *IEEE Trans. Pattern Anal. Mach. Intell.* 39 (9) (2017) 1811–1824.
- [59] C. Chao, A. Liaw, L. Breiman, Using random forest to learn imbalanced data University of California, Berkeley 110 2004 <https://statistics.berkeley.edu/sites/default/files/tech-reports/666.pdf>.
- [60] M. Claesen, D.M. Bart, Hyperparameter search in machine learning (2015) <https://arxiv:1502.02127>.
- [61] T.M. Nir, N. Jahanshad, J.E. Villalon-Reina, A.W. Toga, C.R. Jack, M.W. Weiner, P. M. Thompson, ADNI Alzheimer's Disease Neuroimaging Initiative (ADNI) Effectiveness of regional DTI measures in distinguishing Alzheimer's disease, MCI, and normal aging, *Neuroimage Clin.* 3 (2013) 180–195, <https://doi.org/10.1016/j.nicl.2013.07.006>.
- [62] S.M. Smith, M. Jenkinson, H. Johansen-Berg, D. Rueckert, T.E. Nichols, C. E. Mackay, K.E. Watkins, O. Ciccarelli, M.Z. Cader, P.M. Matthews, T.E.J. Behrens, Tract-based spatial statistics: voxelwise analysis of multi-subject diffusion data, *Neuroimage* 31 (4) (2006) 1487–1505.
- [63] M. Daianu, E.L. Dennis, N. Jahanshad, T.M. Nir, A.W. Toga, C.R. Jack, M. W. Weiner, P.M. Thompson, ADNI Alzheimer's disease disrupts rich club organization in brain connectivity networks, *Proc. IEEE Int. Symp. Biomed. Imaging.* (2013) 266–269, <https://doi.org/10.1109/ISBI.2013.6556463>.
- [64] H. Struyfs, W. Van Hecke, et al., Diffusion kurtosis imaging: A possible MRI biomarker for AD diagnosis, *J. Alzheimers Dis.* 48 (2015) 937–948, <https://doi.org/10.3233/JAD-150253>.
- [65] H.I. Suk, D. Shen, Deep learning-based feature representation for AD/MCI classification, *Med. Image Comput. Comput. Assist. Interv.* 16 (2013) 583–590, https://doi.org/10.1007/978-3-642-40763-5_72.
- [66] H.-I. Suk, S.-W. Lee, D. Shen, Latent feature representation with stacked auto-encoder for AD/MCI diagnosis, *Brain Struct. Funct.* 220 (2) (2015) 841–859.
- [67] H.-I. Suk, S.-W. Lee, D. Shen, Deep sparse multi-task learning for feature selection in Alzheimer's disease diagnosis, *Brain Struct. Funct.* 221 (5) (2016) 2569–2587.
- [68] S. Tax, et al., Prevalence of white matter pathways coming into a single diffusion MRI voxel orientation: the bottleneck issue in tractography, *bioRxiv* (2021), <https://doi.org/10.1101/2021.06.22.449454>.
- [69] G. Girard, M. Descoteaux, Anatomical tissue probability priors for tractography, *Int. Conf. CDMRI* (2012) 174–185.
- [70] A. Lemkaddem, D. Skiöldbrand, A. Dal Palú, J.P. Thiran, A. Daducci, Global tractography with embedded anatomical priors for quantitative connectivity analysis, *Front. Neurol.* 5 (2014) 232, <https://doi.org/10.3389/fneur.2014.00232>.
- [71] C.H. Yeh, R.E. Smith, T. Dhollander, A. Connelly, Mesh-based anatomically-constrained tractography for effective tracking termination and structural connectome construction, *Proc. ISMRM* (2017) 58.
- [72] D.K. Jones, T.R. Knösche, R. Turner, White matter integrity, fiber count, and other fallacies, *NeuroImage* 73 (2013) 239–254.
- [73] K. Schilling, Y. Gao, V. Janve, I. Stepniowska, B.A. Landman, A.W. Anderson, Confirmation of a gyral bias in diffusion MRI fiber tractography, *Hum. Brain Mapp.* 39 (2018) 1449–1466, <https://doi.org/10.1002/hbm.23936>.
- [74] Y. Wu, Y. Hong, Y. Feng, D. Shen, P.T. Yap, Mitigating gyral bias in cortical tractography via asymmetric fiber orientation distributions, *Med. Image Anal.* 59 (2020), 101543, <https://doi.org/10.1016/j.media.2019.101543>.
- [75] D.C. Van Essen, S. Jbabdi, S.N. Sotiropoulos, C. Chen, K. Dikranian, T. Coalson, J. Harwell, T.E. Behrens, M.F. Glasser, Chapter 16 - mapping connections in humans and non-human primates: Aspirations and challenges for diffusion imaging, in: H. Johansen-Berg, T.E. Behrens (Eds.), *Diffusion MRI* (Second Edition), Academic Press, San Diego, 2014, pp. 337–358, <https://doi.org/10.1016/B978-0-12-396460-1.00016-0>.
- [76] M. Ocampo-Pineda, S. Schiavi, F. Rheault, G. Girard, L. Petit, M. Descoteaux, A. Daducci, Hierarchical microstructure informed tractography, *Brain Connect.* 11 (2) (2021) 75–88.
- [77] S. Schiavi, M. Ocampo-Pineda, M. Barakovic, L. Petit, M. Descoteaux, J.P. Thiran, A. Daducci, A new method for accurate in vivo mapping of human brain

- connections using microstructural and anatomical information, *Sci. Adv.* 6 (2020), <https://doi.org/10.1126/sciadv.aba8245>.
- [78] E. Mandonnet, S. Sarubbo, L. Petit, The nomenclature of human white matter association pathways: proposal for a systematic taxonomic anatomical classification, *Front. Neuroanat.* 12 (2018) 94, <https://doi.org/10.3389/fnana.2018.00094>.
- [79] E. Bullmore, O. Sporns, The economy of brain network organization, *Nat. Rev. Neurosci.* 13 (2012) 336–349, <https://doi.org/10.1038/nrn3214>.
- [80] F. Rheault, A. De Benedictis, A. Daducci, C. Maffei, C.M.W. Tax, D. Romascano, E. Caverzasi, F.C. Morency, F. Corrivetti, F. Pestilli, G. Girard, G. Theaud, I. Zemmoura, J. Hau, K. Glavin, K.M. Jordan, K. Pomiecko, M. Chamberland, M. Barakovic, N. Goyette, P. Poulin, Q. Chenot, S.S. Panesar, S. Sarubbo, L. Petit, M. Descoteaux, Tractostorm: the what, why, and how of tractography dissection reproducibility, *Hum. Brain Mapp.* 41 (7) (2020) 1859–1874.
- [81] S. Wakana, A. Caprihan, M.M. Panzenboeck, J.H. Fallon, M. Perry, R.L. Gollub, K. Hua, J. Zhang, H. Jiang, P. Dubey, A. Blitz, P. van Zijl, S. Mori, Reproducibility of quantitative tractography methods applied to cerebral white matter, *Neuroimage* 36 (3) (2007) 630–644.
- [82] C.M. Tax, W.M. Otte, M.A. Viergever, R.M. Dijkhuizen, A. Leemans, REKINDLE: Robust extraction of kurtosis INDices with linear estimation, *Magn. Reson. Med.* 73 (2015) 794–808, <https://doi.org/10.1002/mrm.25165>.
- [83] J. Veraart, E. Fieremans, I.O. Jelescu, F. Knoll, D.S. Novikov, Gibbs ringing in diffusion MRI, *Magn. Reson. Med.* 76 (2016) 301–314, <https://doi.org/10.1002/mrm.25866>.
- [84] E. Kellner, B. Dhital, V.G. Kiselev, M. Reisert, Gibbs-ringing artifact removal based on local subvoxel-shifts, *Magn. Reson. Med.* 76 (2016) 1574–1581, <https://doi.org/10.1002/mrm.26054>.
- [85] B. Ades-Aron, J. Veraart, P. Kochunov, S. McGuire, P. Sherman, E. Kellner, D. S. Novikov, E. Fieremans, Evaluation of the accuracy and precision of the diffusion parameter ESTimation with gibbs and Noise removal pipeline, *Neuroimage* 183 (2018) 532–543.
- [86] R.N. Henriques, S.N. Jespersen, D.K. Jones, J. Veraart, Towards more robust and reproducible diffusion kurtosis imaging, *Magn. Reson. Med.* 86 (2021) 1600–1613, <https://doi.org/10.1002/mrm.28730>.